

Research Article: New Research | Sensory and Motor Systems

Encoding of global visual motion in the avian pretectum shifts from a bias for temporal-to-nasal selectivity to omnidirectional excitation across speeds

<https://doi.org/10.1523/ENEURO.0301-24.2024>

Received: 4 July 2024

Revised: 20 October 2024

Accepted: 22 October 2024

Copyright © 2024 Dash et al.

This is an open-access article distributed under the terms of the [Creative Commons Attribution 4.0 International license](#), which permits unrestricted use, distribution and reproduction in any medium provided that the original work is properly attributed.

This Early Release article has been peer reviewed and accepted, but has not been through the composition and copyediting processes. The final version may differ slightly in style or formatting and will contain links to any extended data.

Alerts: Sign up at www.eneuro.org/alerts to receive customized email alerts when the fully formatted version of this article is published.

1 Systems/Circuits

2 Encoding of global visual motion in the avian
3 pretectum shifts from a bias for temporal-to-
4 nasal selectivity to omnidirectional excitation
5 across speeds

6 **Suryadeep Dash^{1,*†}, Vikram B. Baliga^{1,†}, Anthony B. Lapsansky¹,**
7 **Douglas R. Wylie², and Douglas L. Altshuler¹**

8 ¹Department of Zoology, University of British Columbia, Vancouver, British Columbia V6T 1Z4

9 ²Department of Biological Sciences, University of Alberta, Edmonton, AB, Canada T6G 2E9

10 *current address: Department of Physiology, The Institute of Medical Sciences and Sum Hospital, Siksha
11 'O' Anusandhan University, Odisha, India

12 †co-lead authors

13 Author contributions: S.D., D.R.W., and D.L.A. designed research; S.D. and A.B.L. performed
14 research; V.B.B. analyzed data; D.R.W., V.B.B., and D.L.A. wrote the paper; All authors edited
15 the paper. This work was supported by CIHR Grants FRN 159751 and PJT-169033 to D.R.W.
16 and D.L.A. The authors declare no competing financial interests. Correspondence should be
17 addressed to Douglas R. Wylie at dwylied@ualberta.ca or Douglas L. Altshuler at
18 doug.altshuler@ubc.ca.

19 **Abstract**

20 The pretectum of vertebrates contains neurons responsive to global visual motion. These
21 signals are sent to the cerebellum, forming a subcortical pathway for processing optic flow.
22 Global motion neurons exhibit selectivity for both direction and speed, but this is usually
23 assessed by first determining direction preference at intermediate velocity (16-32 deg/sec),
24 and then assessing speed tuning at the preferred direction. A consequence of this approach
25 is that it is unknown if and how direction preference changes with speed. We measured
26 directional selectivity in 114 pretectal neurons from 44 zebra finches (*Taeniopygia guttata*)
27 across spatial and temporal frequencies, corresponding to a speed range of 0.062 to
28 1024°/s. Pretectal neurons were most responsive at 32-64°/s with lower activity as speed
29 increased or decreased. At each speed, we determined if cells were directionally-selective,
30 bidirectionally-selective, omnidirectionally responsive, or unmodulated. Notably, at 32°/s,
31 60% of the cells were directionally selective and 28% were omnidirectionally responsive. In
32 contrast, at 1024°/s, 20% of the cells were directionally selective and nearly half of the
33 population was omnidirectionally responsive. Only 15% of the cells were omnidirectionally
34 excited across most speeds. The remaining 85% of the cells had direction tuning that
35 changed with speed. Collectively, these results indicate a shift from a bias for directional
36 tuning at intermediate speeds of global visual motion to a bias for omnidirectional responses
37 at faster speeds. These results suggest a potential role for the pretectum during flight by
38 detecting unexpected drift or potential collisions, depending on the speed of the optic flow
39 signal.

40 **Significance Statement**

41 During locomotion, images of edges and surfaces in the environment move across the retina, a
42 signal of global visual motion called optic flow. Retinal recipient areas in the accessory optic
43 system and the pretectum are the earliest sites to encode this signal, and the neurons are
44 selective for direction and speed. Previous work suggested that directional selectivity may
45 change across speeds but this has never been systematically studied. We measured direction
46 preferences from 0.062 to 1024°/s in the avian pretectum. We found that pretectal global motion
47 neurons are biased for temporal-to-nasal motion at intermediate speeds but biased for
48 omnidirectional responses at faster speeds. These results suggest the pretectum could function
49 to detect both unexpected drift and potential collisions during locomotion.

50 **Introduction**

51 As an animal moves through the world, the surfaces and edges in the environment appear to
52 move across the retina, generating a global visual signal known as optic flow (Gibson, 1954).
53 Global visual motion is first encoded primarily as a monocular signal in two regions of the
54 midbrain, the Accessory Optic System (AOS) and the pretectum (Karten et al., 1977; Gamlin
55 and Cohen, 1988; Graf et al., 1988; Soodak and Simpson, 1988). Neurons from these regions
56 exhibit selectivity for direction and speed, but each midbrain site differs in overall population
57 biases. The AOS tends to select for slower speeds (mean typically < 10°/s) and has a region of
58 neurons that prefer upward motion, a region that prefers downward motion, and, in some taxa, a
59 region that prefers backwards (nasal-to-temporal, NT) motion (Simpson et al., 1979; Burns and
60 Wallman, 1981; Grasse and Cynader, 1984; Rosenberg and Ariel, 1990). The pretectum, in
61 contrast, has a bias for faster speeds (mean typically > 10°/s) and for forwards (temporal-to-
62 nasal, TN) motion (Collewijn, 1975; Hoffmann and Schoppmann, 1981; Winterson and Brauth,

63 1985). Both the AOS and pretectum project to the cerebellum and have a role in optokinetic
64 nystagmus (Gioanni et al., 1983, 1984; Simpson et al., 1988a; Lisberger and Sejnowski, 1992;
65 Robinson and Fuchs, 2001). These pathways are also hypothesized to have a role in whole
66 body stabilization and control (Simpson, 1984; Gutiérrez-Ibáñez et al., 2023).

67 In addition to direction selective cells, two other response types have been described in the
68 avian pretectum: bidirectional cells, which respond primarily to opposite directions, and
69 omnidirectional cells, which respond equally well to all directions (Fu et al., 1998; Wylie and
70 Crowder, 2000). A close examination of Wylie and Crowder suggests that direction selectivity
71 could be speed dependent, and a similar argument has been made for the wallaby pretectum
72 (Ibbotson and Mark, 1994). Changes in direction preference were tested across three speeds
73 (6, 15, and 25°/s) in the pretectum of frogs (Fite et al., 1989). Neurons were selective for speed,
74 but did not shift in direction preferences. A broader range of speeds (~ 1-240°) was tested for
75 directional responses in area MT of macaques with a moving bar or spot (Rodman and Albright,
76 1987). Direction preferences were maintained across speeds, but MT neurons have narrower
77 receptive fields compared to global motion neurons in the AOS, pretectum, and macaque MST
78 (Born and Bradley, 2005). Thus, whether directional selectivity is speed dependent has not
79 been systematically tested for neurons responsive to global visual motion across a broad range
80 of speeds.

81 In previous electrophysiological measurements from neurons in the AOS and pretectum, visual
82 stimulus direction and speed were limited for two reasons. The first was that in the initial studies
83 of these regions, stimulus speeds had an upper limit of ~100°/s due to technical constraints
84 (Wylie and Frost, 1990). One solution was to shift from dot field stimulus or gratings with a fixed
85 spatial frequency to gratings that sampled the broader spatiotemporal domain (Wylie and
86 Crowder, 2000). By using combinations of gratings that varied in spatial and temporal
87 frequency, stimulus speeds could be tested up to ~1000 °/s (Smyth et al., 2022). The second
88 limitation was that there are a large number of combinations of directions and speeds. In
89 previous studies, the solution was to fix direction by first determining the preferred direction at
90 one speed, and then to test how the cell responded across a range of speeds. Speed tuning has
91 generally been evaluated only in each cell's preferred, and in some cases anti-preferred
92 directions.

93 Here we ask if both stimulus direction and speed are varied, does directional selectivity change
94 across speeds. We performed extracellular recordings from the pretectal nucleus lentiformis
95 mesencephali (LM) in zebra finches (*Taeniopygia guttata*). The avian LM is homologous to the
96 mammalian NOT (Fite, 1985; McKenna and Wallman, 1985). We tested cells in the
97 spatiotemporal domain, but used a restricted set of grating stimuli that maximized the range of
98 tested velocities.

99 **Materials and Methods**

100 The study subjects were 44 adult male zebra finches (*Taeniopygia guttata*). All procedures were
101 approved by the University of British Columbia Animal Care Committee in accordance with the
102 guidelines set by the Canadian Council on Animal Care.

103 *Surgical and electrophysiological recording procedures*

104 Animals were anesthetized by an intramuscular injection of 65 mg/kg of ketamine and 8 mg/kg
105 of xylazine. Supplemental doses were delivered when the bird exhibited any reflexive
106 movements. Once birds were in the surgical plane, as assessed via the absence of pedal
107 withdraw reflex, they were placed in a custom small bird stereotax (Herb Adams Engineering,
108 Glendora, CA). The head were secured with ear bars and by clamping the beak on an
109 adjustable arm. The arm was pitched downward 45° relative to the horizontal plane. A
110 subcutaneous injection of 150 μ L of 0.9% NaCl solution was made if needed to help the
111 maintain hydration and ion balance during surgery. An incision was made to expose the dorsal
112 surface of the skull. A glass pipette with a tip diameter of \sim 5 μ m was filled with a 2M NaCl
113 solution and mounted on a motorized micromanipulator. The pipette was moved to the location
114 of the y-sinus. The initial coordinate for the center of the pretectal nucleus lentiformis
115 mesencephali (LM) at this stereotaxic head angle is 2.8 mm anterior and 2.5 mm lateral right to
116 the y-sinus. The right LM was targeted because it receives contralateral projections from the left
117 eye, which was the location of stimulus presentation.

118 A ground electrode was attached under the skin near the incision position on the head. The
119 electrode and ground were connected via head stage to a single channel amplifier (A-M
120 Systems Inc., Sequim, WA, Model 3000) with a gain of 10,000 and the filters set wide open.
121 Amplified signals were delivered to an audio monitor (A-M Systems Inc., Model 3300) and also
122 to an analog-to-digital acquisition (DAQ) system (CED, Cambridge, UK, micro1401-3).

123 The feathers below the left eye were lightly taped to the ear bar to keep the eye open. Pretectal
124 LM neurons in the zebra finch were targeted using a stereotaxic atlas (Nixdorf-Bergweiler and
125 Bischof, 2007). The electrode was lowered while monitoring the recording. We showed global
126 visual motion to the open eye, either through movement of a large board with complex visual
127 patterns or by placing a video screen in the eye's path while displaying in multiple directions and
128 at multiple speeds. When we encountered a cell that responded to these stimuli, we made an
129 initial assessment as to whether the recorded neuron was pretectal or tectal. The key difference
130 is that pretectal LM neurons respond to moving large-field motion unlike nearby tectal cells,
131 which only respond to small stimuli (Frost et al., 1990). A putative LM neuron was identified
132 when the response was sustained in at least one direction. In this stereotaxic coordinate
133 system, the LM is typically reached at a depth between 5.1 and 7.9 mm. Once a putative LM
134 neuron was identified, the electrode was adjusted to maximize isolation (Figure 1B).

135 *Stimulus presentation and data acquisition*

136 Two different spatiotemporal stimulus programs were used to study cell responses across a
137 range of visual motion speeds (Figure 1C). In all cases, a stimulus sweep consisted of a blank
138 screen for 1s, followed by a static black and white sine wave grating for 1s, which was followed
139 by that same sine wave grating in motion for 3s. The computer that generated the stimulus sent
140 a TTL pulse with each sweep that was acquired in the DAQ and synchronized with the
141 electrophysiological data. A photodiode, attached to the lower corner of the stimulus screen,
142 simultaneously verified the timing of stimulus changes. Eight directions were tested, 45° apart.
143 In our stimulus program, 0° and 180° were aligned with the stereotaxic arm. Based on high-
144 speed video recording of a zebra finch in flight, we determined that the earth horizontal (nasal-
145 temporal) plane for a zebra finch is 20° above a bird's orientation in the stereotax. We define
146 temporal-to-nasal (TN) direction as 0°, the "down" direction as 90°, the nasal-to-temporal

147 direction as 180°, and the “up” direction as 270°. In this coordinate system, the
148 electrophysiological measurements were made at stimulus direction of 20°, 65°, 110°, 155°,
149 200°, 245°, 290°, and 335°. In the first set of experiments, spatial frequency ranged from 0.0155
150 to 0.5 cycles per degree (cpd) and temporal frequency ranged from 0.031 to 16 Hz. Six speeds
151 were tested: 0.062, 0.5, 4, 32, 256, and 1024 °/s. These stimuli were programmed using
152 Psychophysics Toolbox3 in MATLAB. For each cell recording, the full set of stimuli were
153 ordered randomly and tested once each, which defined a full stimulus sweep. Up to ten full
154 stimulus sweeps were performed.

155 During this first set of experiments, we found that responses at the low speeds (< 4°/s) were
156 often indistinguishable from the spontaneous rate. We therefore designed a new stimulus
157 program to gain further resolution of response differences at faster speeds. The spatial
158 frequencies ranged from 0.0155 to 0.25 cpd, and the temporal frequencies ranged from 1 to 16
159 Hz. Up to ten speeds were tested: 4, 8, 16, 32, 64, 128, 256, 407, 644, and 1024 °/s. All cells in
160 both sets of experiments were tested at 4, 32, 256, and 1024 °/s. We confirmed with high-speed
161 video recording (512 frames per second) that there was no aliasing at any stimulus speed.

162 Electrophysiological data were acquired and initial analysis was performed using Spike2
163 (Cambridge Electronic Design; Cambridge, UK). Raw traces were sorted into single units with
164 isolated spikes (wavemarks) using full-wave templates. The template window width was set to
165 include a full spike and trigger thresholds were adjusted to exclude noise and capture spikes.
166 Spike sorted data were exported in Matlab (MathWorks; Natick, USA) format for further
167 analysis.

168 *Cell classification*

169 We generated a diagnostic analysis for each cells’ responses, which included raster plots, peri-
170 stimulus time histograms, and polar tuning plots (Figure 2). This initial analysis revealed
171 transient activity as the stimulus changed from blank screen to stationary stimulus to moving
172 stimulus and back to blank screen. The transient responses lasted up to 200 ms. We calculated
173 the spontaneous firing rate for each cell as the average response during the period of 500-1000
174 ms when all of the stationary stimulus patterns were displayed. We next calculated the average
175 response to moving stimuli for each sweep at a given speed and direction over the motion
176 epoch. At this stage, some cells were excluded from further analysis because they did not meet
177 criteria for being selective for global visual motion. The inclusion criteria required that cell
178 exhibited the following for at least one speed: 1) a sustained response to at least one stimulus
179 condition across sweeps; 2) a response to at least one direction with a firing rate greater than or
180 equal to 5 spikes/s above the spontaneous firing rate. Following diagnostic checks, we had a
181 total sample of 114 neurons, and total sample of 924 cell responses across speeds (Figure 1C
182 inset).

183 We next generated polar tuning plots and fitted a natural cubic spline to these data, with 7 or 8
184 degrees of freedom. The polar tuning plots revealed that the responses could be categorized
185 based on the shape of the curves. A curve with a single prominent peak illustrates a “directional”
186 preference. Some curves had two peaks, typically 180° apart, and therefore represent
187 “bidirectional” activity. We also noticed that some cells were responsive to all directions of
188 motion, which we termed “omnidirectional”. Finally, some cells that were active at one or more

189 speeds were unresponsive to any direction of global visual motion at other speeds. We term this
190 lack of response as “unmodulated”.

191 To aid in the classification of the 924 cell responses at each stimulus speed, we calculated
192 several response properties. For all of these response properties, we subtracted the mean
193 spontaneous rate from the firing rate in response to a visual stimulus. The preferred direction of
194 each cell at each speed was calculated using the vector sum:

$$195 \quad \textit{Preferred direction} = \tan^{-1} \left(\frac{\sum_n (FR_n * \sin\theta_n)}{\sum_n (FR_n * \cos\theta_n)} \right)$$

196 where FR = firing rate and n = the eight directions of motion in radians.

197 Tuning properties of LM neurons were characterized using four other parameters. The width of
198 the direction tuning curve was calculated using the sensitivity index (SI), which is defined as
199 normalized length of the mean response vector (Vogels and Orban, 1994):

$$200 \quad SI = \frac{\sqrt{(FR_n * \sin\theta_n)^2 + (FR_n * \cos\theta_n)^2}}{\sum_n FR_n}$$

201 where FR_n is the average firing rate in response to direction n for all eight directions of motion
202 presented (in radians). The SI ranges from 0 to 1, with an SI of 0 indicating a neuron responding
203 equally to all measured directions of motion, and an SI of 1 indicating that a neuron responds
204 only to a single motion direction. Another measure of the strength of direction tuning is the ratio
205 of the firing rate in the anti-preferred direction to the firing rate in the preferred direction
206 (AP/PD). The AP is opposite (180° away) from the PD. We also calculated the ratio of the mean
207 of the firing rate across all directions to the standard deviation of the average firing rates to each
208 direction. This measure is higher for cells that are responsive to many directions and is the
209 inverse of the coefficient of variation (Inverse CV). Finally, we implemented the findpeaks
210 function in *pracma* (Borchers, 2023) to determine the peak count.

211 Cell responses at each speed were classified based on the shape of the turning curves using a
212 machine learning approach. To establish a training data set, we focused on classifying the
213 response of each cell at the speed at which the cell's response was most active (i.e., the speed
214 at which the response in the preferred direction was greatest vs. the cell's spontaneous rate). In
215 these “most active” conditions, all 114 cells exhibited activity above spontaneous firing rate, and
216 could be manually classified into one of three categories: bidirectional, directional, or
217 omnidirectional. Our manual classifications generally relied on assessing the overall shape of
218 the tuning curve but were also aided by whether SI was > 0.2, which was generally indicative of
219 directional classification. To ensure the training data set was not systematically biased by the
220 most active responses, we manually classified an additional 100 modulated responses,
221 choosing cells and speeds randomly. In an initial approach, we had included cell responses that
222 were “unmodulated” as a potential category but found doing so resulted in poor performance
223 (high misclassification rate). This was likely due to unmodulated responses having tuning curves
224 that could be similar in shape to those of directional, omnidirectional, or bidirectional responses,
225 albeit at an overall lower spike rate. We therefore elected to perform two stages of analysis: 1)

226 categorize all responses based on the shape of the tuning curve using machine learning and 2)
227 re-classify some responses as unmodulated based on additional criteria.

228 In the first stage of classification, we used extreme gradient boosting via XGBoost (Chen and
229 Guestrin, 2016). Boosting is an ensemble extension of random forest modeling: decision trees
230 are fit to training data sequentially to improve upon preceding outcomes. An example of a
231 decision tree that could have been used during boosting is shown in figure 3A. The target
232 variable for the model was the manually classified responses from the training data set. The
233 features included SI, inverse CV, AP/PD, and peak count. To improve generalizability, we
234 performed repeated k-fold cross-validation, with 5 repeats and with $k = 5$. Additional details of
235 the tuning grid, including boosting rounds, eta, gamma, and subsampling are available in our
236 code repository (Baliga et al., 2024). The best-tuned model was determined and found to have
237 100% accuracy on the training data set (Chi-sq: 426, $p < 0.001$) as well as on several test data
238 sets. The parameters of SI and inverse CV were the most informative for the model, both in
239 terms of their relative contributions (gain) and relative number of observations (cover) (Figure
240 3B). The parameters of peak count and AP/PD provided further refinement. This model was
241 subsequently used to predict the categorization of all 924 cellular responses (Figure 3D-G,
242 Figure 3-1). Response classifications were thereafter spot-checked and, in all cases, found to
243 agree with manual classification.

244 In stage 2, we re-classified some responses as unmodulated (Figure 3C). A cell's response can
245 be considered unmodulated if it is not sufficiently distinguishable from the cell's spontaneous
246 rate. We applied a rule wherein two conditions were checked: 1) whether a cellular response
247 was not statistically different from the spontaneous rate in more than 6 directions, and 2) if $SI <$
248 0.29 . If both conditions were true, the cell response was re-classified as unmodulated.

249 *Data analysis*

250 To facilitate comparisons of how LM directions responses changed with speed, we normalized
251 firing rates within cells and across speeds. Data within each cell were normalized to the
252 absolute value of the maximum response among all speeds and directions. This defines R_n , the
253 "normalized directional response", as ranging from -1 (maximal possible suppression) to +1
254 (maximum response recorded). Because the spontaneous firing rate had already been
255 subtracted prior to this normalization, the spontaneous rate was defined as 0 for the normalized
256 response.

257 A response feature that became apparent during diagnostic analysis is that the duration of the
258 responses also varied with speeds. To facilitate analysis of responses through time, we
259 separately normalized firing rates within cells and across time bins to define the "normalized
260 temporal response". At each speed and each direction, the response to the motion epoch was
261 divided into 10 ms bins. The spontaneous rate of the cells was subtracted from each bin. The
262 bins were normalized to the absolute value of the maximum response across all such bins for a
263 given cell. As above, this led to a given cell's maximum response being defined as 1, its
264 spontaneous rate being defined as 0, and its maximum possible level of suppression being
265 defined as -1.

266 Uncertainty bands in figures are 95% confidence intervals, which are used in many cases for
 267 comparisons among fitted curves. Statistical trends in response properties with stimulus speed
 268 were assessed by comparing goodness of fit via AIC among candidate Generalized Additive
 269 Models (GAM). To assess speed tuning we compared among the following three models:

$$270 \quad R_n \sim (1 \mid cell)$$

$$271 \quad R_n \sim s(\log_2(speed))$$

$$272 \quad R_n \sim s(\log_2(speed)) + (1 \mid cell)$$

273 Where s is the GAM smoothing function.

274 In a separate set of analyses, we tested how the time to peak activity ($time_p$) changes with
 275 stimulus speed. Here, the responses over time were compared via AIC using the following five
 276 GAM models:

$$277 \quad \log_2(time_p) \sim (1 \mid cell)$$

$$278 \quad \log_2(time_p) \sim s(\log_2(speed))$$

$$279 \quad \log_2(time_p) \sim s(\log_2(speed)) + (1 \mid cell)$$

$$280 \quad \log_2(time_p) \sim shape + s(\log_2(speed) * shape)$$

$$281 \quad \log_2(time_p) \sim shape + s(\log_2(speed) * shape) + (1 \mid cell)$$

282 Where $shape$ is a discrete variable that can have one of three states: directional, bi-directional,
 283 or omnidirectional. Unmodulated cells were excluded. Separate model fitting was performed for
 284 two data sets: one where data were averaged across all 8 directions, and one where only data
 285 from the direction closest to the preferred direction were used.

286 We also tested how the magnitude of peak activity within each phase ($activity_p$) changes with
 287 stimulus speed. Here, the responses over time were compared via AIC using the following five
 288 GAM models:

$$289 \quad activity_p \sim (1 \mid cell)$$

$$290 \quad activity_p \sim phase + s(\log_2(speed) * phase)$$

$$291 \quad activity_p \sim phase + s(\log_2(speed) * phase) + (1 \mid cell)$$

292 Where $phase$ is a discrete variable that can have one of three states: initial transient,
 293 transitional, or steady state. Again, separate model fitting was performed for two data sets: one

294 where data were averaged across all 8 directions, and one where only data from the direction
295 closest to the preferred direction were used.

296

297 *Code Accessibility*

298 The spike-sorted electrophysiological data and analysis code are available via Figshare (Baliga
299 et al., 2024).

300 **Results**

301 Pretectal LM neurons were most responsive at intermediate speeds (32-64°) and declined at
302 slower and faster speeds (Figure 4). The normalized directional responses are shown grouped
303 by speed in figure 4A. At intermediate speeds, the directional tuning curves tended to be
304 relatively sharp and centered at 0°, which corresponds to temporal-to-nasal (TN) motion. At
305 slower speeds, especially below 4°/s, the neuron responses were considerably reduced. At
306 faster speeds (> 64°), the cells remained active, but the tuning curves were flatter indicating a
307 shift towards omnidirectional responses. Suppression, which is indicated by negative values in
308 the normalized response was relatively infrequent.

309 The mean responses at each speed with the 95% confidence intervals are shown in figure 4B.
310 The TN population bias is strongest at 32 and 64°/s, but also present at 16 and 128°/s. At all
311 speeds > 4°/s, the population shows responses to global visual motion, and at speeds > 128°/s,
312 the population response is relatively uniform across directions. We further examined these
313 differences by aligning all tuning curves at each cell's preferred direction at each speed (Figure
314 4C). Because of the consistently strong bias for TN motion at intermediate speeds and the more
315 uniform responses at faster speeds, this display of speed-specific tuning responses was largely
316 unchanged. The widths of the directional tuning curves are relatively broad, typically spanning
317 more than $\pm 45^\circ$ of the preferred direction.

318 To generate a population speed tuning curve (Figure 4D), we plotted each cell's maximum
319 normalized directional responses at each speed. The best fitting GAM model (Table 1) indicated
320 that cells generally achieved their highest normalized responses around 32°/s and that cell
321 identity did not have meaningful effect on the overall relationship between normalized response
322 and log2 of speed. The speed at which each cell reached its measured maximum response is
323 shown in black in Figure 4E. Because sample size varied due to two different experimental
324 protocols (Figure 1C), we normalized these data to the sample size at each speed (Figure 4F).
325 The majority of zebra finch LM neurons have their highest responses to global visual motion at
326 32°/s.

327 We next asked if preferred directions changed across stimulus speeds. For each cell, we plotted
328 the preferred direction at each measured speed against the preferred direction at each most
329 active speed, depicting its speed-specific classification and SI (Figure 5A). If each cell's
330 preferred direction had been maintained within 45° across speeds, all of the dots would have
331 fallen within the gray region. Of the cells that were sampled at all four common speeds (4, 32,
332 256, 1024°/s), nearly half (46%) of the cellular responses fall within this zone and the other half

333 (54%) are outside of it (Figure 5A inset). LM neurons tend to be directional and prefer TN
334 motion, but these characteristics are most apparent at speeds of 32°/s and to a lesser extent at
335 4°/s (Figure 5B). Relatively few of the cells were directional at faster speeds and there was no
336 overall bias for TN motion among those that are.

337 Because it is clear that direction tuning changed across speeds, we also analyzed how cell
338 classification changes. Examples of cells that maintained directional (Figure 5C) and
339 omnidirectional (Figure 5E) classification across the four common speeds illustrate that
340 response strengths also varied across speeds. A commonly observed pattern was for cells that
341 were directional at intermediate speeds to shift to omnidirectional at faster speeds (Figure 5D).
342 Bi-directional cells were rare and none maintained this classification across speeds. An example
343 of cell that was bidirectional at only 256°/s is shown in Figure 5f. The cells classification for all
344 cells at the four speeds that were commonly tested is shown in a tile plot, with cells are ordered
345 based on classification at 32°/s (Figure 5G). This ordering suggests that responses across
346 speeds can be grouped into four categories. 36 out of 114 neurons were directionally-tuned
347 (green) at 32°/s but shifted to being omnidirectional at 256°/s. The majority remained
348 omnidirectional at 1024°/s. The tuning curves for the 36 cells in this category are shown in figure
349 5H. The next category consists of 32 neurons that are primarily directional. All of these cells
350 were directionally-tuned (green) at 32°/s. Most of them were also directionally-selective at either
351 4°/ or 256°/s, but only four of these were directionally-tuned across all directions (Figure 5I). The
352 third category is for the 24 LM neurons that were omnidirectional at most speeds (J). The last
353 category is composed of 22 cells with variable responses, including cells that were bi-directional
354 at 32°/s. Note that the polar plots in C-F are shown with the radius in spikes/s and the radii of
355 the plots in H-K are normalized to the maximum firing rate of each cell.

356 We have previously demonstrated that the majority of neurons finch LM prefer TN motion at
357 intermediate speeds (Gaede et al., 2017; Smyth et al., 2022), as is the case for most
358 vertebrates. In the current study, 44 of the 114 were both directional and TN tuned at 32°/s. To
359 examine how these cells change in direction tuning across speeds, we made a Sankey diagram
360 (Figure 6A). Only 7 of these cells were directional at 1024°/s and of these, only three of them
361 remained TN selective. The most common pattern was for cells to become omnidirectional at
362 faster speeds. The tendency is also apparent from a second Sankey diagram, which is
363 composed of all 52 cells that were omnidirectional at 1024°/s (Figure 6B). The majority of these
364 (30 out of 52) were directional at 32°/s.

365 A previous study of LM responses to largefield moving stimuli demonstrated that the cells have
366 a strong initial transient followed by a sustained steady-state response (Smyth et al., 2022). This
367 prior result next led us to ask if there are relationships among response stimulus speed and cell
368 response dynamics. We divided the response of each epoch of moving stimuli into an initial
369 transient phase (IT, 40-200 ms), a transitional phase (TR, 200-1000), and a steady-state phase
370 (1000-3000 ms) (Figure 7A). We also consider how these responses compare to the full-time
371 stimulus (FT, 40-3000 ms). Plotting the normalized temporal responses reveals that at the faster
372 stimulus speeds, the initial transient response is predominant (Figure 7B). At intermediate
373 speeds (32-64°/s), the initial transient is also elevated but the steady-state response is
374 maintained. These trends are stronger for the preferred direction (green) but also present in the
375 anti-preferred direction (orange). At slow speeds (<4°/s), responses are minimal. The trends in
376 temporal dynamics are particularly apparent by focusing on the first 500 ms of response for the

377 four common speeds (Figure 7D). The polar plots for all cellular responses are shown for each
378 epoch of stimulus presentation (Figure 7C). The overall population bias for TN motion at
379 intermediate speeds is maintained throughout stimulus presentation. In contrast, the population
380 bias for omnidirectional motion at faster speeds is strongest at the initial transient phase and
381 reduced or absent thereafter.

382 The analyses in figure 7 indicate the temporal dynamics of the response to motion are
383 important. We next asked how long does it take the cells to reach peak activity following the
384 onset of stimulus motion. This value is plotted for all cells at all speeds, either when averaged
385 across all directions (Figure 8A) or when only considered for the direction that was closest to the
386 preferred direction (Figure 8B). Each of best fitting GAMs (Tables 2, 3) indicates that the time to
387 peak normalized activity decreases monotonically as speed increases. These relationships were
388 not affected by the shape of the tuning curve (directional, bi-directional, or omnidirectional).
389 Time to peak activity does decline at a slower rate, however, when considering only the
390 preferred direction.

391 An earlier study of lobula plate tangential cells, specifically H1 cells, of the blowfly demonstrated
392 that the transient response of the cells is biased for faster speeds than the steady response
393 (Maddess and Laughlin, 1985). To determine if a similar phenomenon exists for zebra finch LM
394 neurons, we examined the peak spike rate during the initial transient, transitional, and steady-
395 state responses. The spike rates were normalized to the highest rate shown by each cell, in any
396 direction, across the full motion epochs. When considering the responses averaged across all
397 directions (Figure 8C), the best fitting GAM (Table 4) indicates that the steady responses were
398 consistently low, with a slight peak at intermediate speeds (16-64°/s). The initial transient and
399 transitional phases were more strongly biased for speed, with the peak of the transitional
400 phases biased for intermediate speeds, and the peak of the initial transient biased for faster
401 speeds. When considering only the preferred direction (Figure 8D), the best fitting GAM (Table
402 5) indicated that overall responses were higher, but the transient response was still biased for
403 faster speeds than either the steady-state or transitional responses.

404 Discussion

405 We asked if the directional selectivity of midbrain neurons that respond to global visual motion
406 changes across stimulus speeds. We made single unit recordings from the pretectal nucleus
407 lentiformis mesencephali (LM) of zebra finches (*Taeniopygia guttata*) across a range of stimulus
408 speeds by varying spatial and temporal frequency (Figure 1). Cellular responses to stimulus
409 direction could be characterized as directional, bidirectional, omnidirectional or unmodulated
410 using several metrics (Figure 2). These metrics allowed for automated classification of cellular
411 responses using machine learning (Figure 3, Figure 3-1). LM neurons were most responsive at
412 intermediate stimulus speeds (32-64°/s) (Figure 4). Considering the responses across all
413 speeds, the cells could be grouped into four general categories (Figure 5): cells that 1) shifted
414 from directionally-selective at intermediate speeds to omnidirectionally responsive at faster
415 speeds; 2) were directionally-selective at most speeds; 3) were omnidirectionally responsive at
416 most speeds; 4) were variable in responses across speeds. As in our previous studies of zebra
417 finch LM neurons (Gaede et al., 2017; Smyth et al., 2022), most of the cells were directional at
418 32°/s (n = 68 out of 114 cells) and the majority of those cells (n = 44) preferred temporal-to-
419 nasal motion. We performed further analysis on how those responses in particular changed
420 across speeds (Figure 6). Only seven of the cells that were TN preferring at intermediate

421 speeds remained directional at the fastest speed (1024°/s). Of these cells, only three preferred
422 TN motion at this speed. In contrast, many of the LM neurons were omnidirectionally responsive
423 ($n = 52$ out of 114 cells) at the fastest speed. Thus, we observed an overall shift in the bias of
424 LM neurons for temporal-nasal directional selectivity at intermediate speeds to omnidirectional
425 responsiveness at very fast speeds. Lastly, we analyzed the temporal dynamics of the
426 responses during stimulus motion, which revealed that the response had early onset and rapid
427 offset at high stimulus speed (Figure 7,8). Overall, the measurements from LM neurons identify
428 a previously uncharacterized shift in tuning such that at high speeds, the responses of many
429 cells are rapid, transient, and omnidirectional.

430 Changes in the directional selectivity of pretectal neurons to global visual motion have also been
431 reported in the wallaby NOT (Ibbotson and Mark, 1994). At slow speeds, wallaby NOT neurons
432 preferred TN motion but at high speeds they were inhibited by motion in all directions. It was
433 proposed that this inhibition was mediated by omnidirectional cells in or near the NOT. In
434 contrast, we observed some of the same LM cells shifting from TN selective to omnidirectionally
435 responsive across speeds. Comparison of these results suggests that population responses
436 across speeds in the wallaby NOT and the zebra finch LM arise from different mechanisms.

437 Until very recently, the responses of neurons in the accessory optic system and pretectum to
438 global visual motion from a diversity of animals were only tested at stimulus speeds up to
439 512°/s, and in most cases the upper limit was closer to 100°/s. The resulting speed tuning
440 curves have peak responses at values less than 100°/s. The first study of LM neurons in
441 hummingbirds used random dot field stimuli that had a maximum stimulus speed of 80°/s
442 (Gaede et al., 2017). This study was designed to test the hypothesis proposed by Iwaniuk and
443 Wylie (Iwaniuk and Wylie, 2007) that the hypertrophied LM of hummingbirds would have a bias
444 for slower speeds. In contrast, hummingbirds were found to have a bias for faster speeds
445 although the values for the peak responses could not be identified for many cells as they were
446 clearly above the upper limit for the stimulus. These results inspired us to shift from using dot
447 field stimulus to sine wave gratings that could be varied in spatial and temporal frequency
448 (Smyth et al., 2022). Across the full spatiotemporal domain, this approach has an upper limit of
449 1024°/s for the applied stimuli. Some cells from both zebra finches and Anna's hummingbirds
450 (*Calypste anna*) were found to have peak responses above 100°/s. These responses, however,
451 were only tested in the preferred direction due to the constraints of holding neurons across the
452 full range of stimulus treatments to fully sample the spatiotemporal domain. The approach for
453 the current study was to use a narrow set of spatial and temporal frequency stimulus
454 combinations to maximize sampling across stimulus speeds, but to test directional responses at
455 each speed.

456 In the LM of pigeons and in the NOT of mammals, the cells can be divided into a slow and a fast
457 population, often with the cutoff of 4°/s (Ibbotson and Price, 2001; Winship et al., 2006). Of the
458 animals studied so far, hummingbirds and zebra finches are different in that LM neurons with
459 peak responses at speeds $< 4^\circ/\text{s}$ are rare. In the current data set, none of the zebra finch LM
460 neurons had peak responses at slow speeds. Ibbotson and Price (Ibbotson and Price, 2001)
461 have argued that fast neurons would be responsible for the initial phase of optokinetic
462 nystagmus when the retinal slip velocity is high, and the slow neurons are responsible for
463 driving optokinetic nystagmus when retinal slip velocities are low. It seems unlikely that zebra
464 finches lack the ability to follow motion stimuli. As can be seen in figure 8D, LM neurons in the

465 zebra finch do respond to slow velocities ($<4^\circ/s$), especially in the preferred direction albeit be a
466 lower gain compared to the peak response. Thus, in zebra finches, responses to both slow and
467 fast OKN may be accomplished by some of the same cells, but with different temporal
468 dynamics.

469 Global visual motion is also analyzed in other subcortical regions in vertebrates. The accessory
470 optic system contains populations of neurons that prefer either upward or downward motion,
471 and in some species, there is also a small population of NT preferring cells (McKenna and
472 Wallman, 1985; Simpson et al., 1988b; Soodak and Simpson, 1988; Wylie and Frost, 1990;
473 Gaede et al., 2022). Both the pretectum and the accessory optic system sends strong
474 projections to the vestibulocerebellum, both through mossy fibre projections and climbing fibre
475 projections through the inferior olive (Simpson, 1984; Wylie, 2000; Pakan et al., 2010). In
476 mammals and in pigeons, the vestibulocerebellum is arranged into bands of selectivity for
477 panoramic visual fields with different optic flow tuning (Graf et al., 1988; Kano et al., 1990;
478 Kusunoki et al., 1990; Wylie et al., 1993). The general vertebrate pattern of anatomical
479 connectivity has been confirmed in zebra finches (Gaede et al., 2019; Wylie et al., 2023).
480 Because we are currently lacking measurements of neurons in the zebra finch
481 vestibulocerebellum to global visual motion, it is unknown how these may be affected by speed-
482 dependent changes in the directional selectivity of pretectal neurons.

483 Although LM is only one component of the midbrain-cerebellar pathway for optic flow
484 processing, it is nonetheless worthwhile to consider what role it could have in flight control. In
485 the zebra finch, the LM has a strong bias for temporal-to-nasal motion at intermediate stimulus
486 speeds (Gaede et al., 2017; Smyth et al., 2022), whereas the nucleus of the basal optic root has
487 a bias for upwards and downwards motion (Gaede et al., 2022). This division of direction
488 preferences is generally consistent across vertebrates (Simpson et al., 1979; Burns and
489 Wallman, 1981; Hoffmann and Schoppmann, 1981; Grasse and Cynader, 1984; Fite, 1985;
490 McKenna and Wallman, 1985; Winterson and Brauth, 1985; Mustari and Fuchs, 1990;
491 Rosenberg and Ariel, 1990; Ibbotson et al., 1994; Wylie and Crowder, 2000; Wylie, 2013).
492 Given the bias of LM and its mammalian homolog for horizontal optic flow, and temporal-to-
493 nasal motion in particular, why is there no major population of neurons in the midbrain for
494 responses to nasal-to-temporal motion? It has been proposed that because this pathway is
495 involved in stabilizing visual reflexes, it would be detrimental to have strong oculomotor
496 responses to nasal-to-temporal motion given that this is the primary direction of optic flow during
497 forward movement through the environment (Collewijn and Noorduyn, 1972; Land, 2015). An
498 alternative, non-exclusive hypothesis is that heightened sensitivity to temporal-to-nasal motion
499 could be particularly beneficial stabilizing whole body locomotion by allowing animals to detect
500 unwanted backwards drift due to wind or water currents (Chapman et al., 2011). The only
501 animal group documented so far that lacks an overall temporal-to-nasal bias in the pretectum in
502 the hummingbird, which also is unique among vertebrates in its ability to sustain hovering flight
503 (Gaede et al., 2017; Smyth et al., 2022). This result suggests to us that the direction and speed
504 tuning in the midbrain-cerebellar optic flow pathways may have functional consequences for
505 locomotor control in addition to their well-described role for eye stabilization.

506 Does the shift in bias from TN tuning to omnidirectional responses have a functional implication
507 for zebra finch flight control? A distinct feature of optic signals is that optic flow velocity
508 increases with proximity to a surface or edge in the environment (Gibson, 1954; Ibbotson,

509 2017). The population of LM neurons in the zebra finch is therefore expected to become very
510 active as a bird flies very close to objects in its environment, even though this activity should
511 have little if any directional signal. At very fast speeds, it may be challenging for the visual signal
512 to encode direction accurately due to temporal dynamics of local motion detecting circuits and
513 aliasing. It may also be that a proximity signal transmitted by the LM population does not need
514 to have directional information to be useful for collision avoidance.

515 A well-known proximity signal in animal visual systems is the response to looming, especially to
516 an expanding OFF stimulus (Klapoetke et al., 2017; Kim et al., 2020). Encoding of looming has
517 been demonstrated in the tectofugal pathway of birds (Sun and Frost, 1998). We are not aware
518 of any data suggesting that the accessory optic system and/or pretectum also contains looming-
519 sensitive cells but it may also be that looming stimuli have not been tested at sufficiently fast
520 speeds to elicit such a response.

521 The hypothesis that LM neurons function as a warning system, signaling unexpected backwards
522 drift at intermediate optic flow velocity, and signaling dangerous proximity at very fast optic flow
523 velocity could be tested during locomotion. If a flying zebra finch experiences temporal-to-nasal
524 optic flow at intermediate speeds, it is expected to make a compensatory movement as it
525 attempts to negate this regressive optic flow. It is predicted that this response will be abolished if
526 the population of LM neurons that are TN preferring at intermediate speeds is inactivated
527 pharmacologically or optogenetically. If a flying zebra finch experiences very fast optic flow,
528 regardless of direction, it is expected to make a rapid avoidance response. Our data suggest
529 that such a response would be driven by the initial transient response of the omnidirectionally-
530 sensitive LM neurons. It is therefore predicted that if this population of LM neurons could be
531 briefly silenced during the first ~200 ms of a fast omnidirectional stimulus presentation, any
532 avoidance response should be eliminated or reduced. All of these predictions are based on the
533 hypothesis that diverse response properties of the same LM neurons can be processed
534 differently in downstream regions such as the cerebellum.

535 **Acknowledgments**

536 This work was supported by CIHR Grants FRN 159751 and PJT-169033 to D.R.W. and D.L.A.
537 We thank Eshan Nirody for assistance with stimulus code and Sylvia Heredia for the illustration
538 in figure 1A.

539 **References**

- 540 Baliga VB, Dash S, Lapsansky AB, Wylie DR, Altshuler DL (2024) Data and code for “Encoding
541 of global visual motion in the pretectum shifts from a bias for temporal-to-nasal
542 selectivity to omnidirectional excitation across speeds.” Available at:
543 <https://figshare.com/s/47757e81d2db3d75a340>.
- 544 Borchers HW (2023) pracma: practical numerical math functions. Available at: [https://cran.r-
545 project.org/web/packages/pracma/index.html](https://cran.r-project.org/web/packages/pracma/index.html).
- 546 Born RT, Bradley DC (2005) Structure and function of visual area MT. *Annu Rev Neurosci*
547 28:157–189.

548 Burns S, Wallman J (1981) Relation of single unit properties to the oculomotor function of the
549 nucleus of the basal optic root (accessory optic system) in chickens. *Exp Brain Res*
550 42:171–180.

551 Chapman JW, Klaassen RHG, Drake VA, Fossette S, Hays GC, Metcalfe JD, Reynolds AM,
552 Reynolds DR, Alerstam T (2011) Animal orientation strategies for movement in flows.
553 *Current Biology* 21:R861–R870.

554 Chen T, Guestrin C (2016) XGBoost: a scalable tree boosting system. In: Proceedings of the
555 22nd ACM SIGKDD International Conference on Knowledge Discovery and Data Mining,
556 pp 785–794. San Francisco California USA: ACM.

557 Collewijn H (1975) Direction-selective units in the rabbit's nucleus of the optic tract. *Brain Res*
558 100:489–508.

559 Collewijn H, Noorduyn H (1972) Conjugate and disjunctive optokinetic eye movements in the
560 rabbit, evoked by rotatory and translatory motion. *Pflugers Arch* 335:173–185.

561 Fite KV (1985) Pretectal and accessory-optic visual nuclei of fish, amphibia and reptiles: theme
562 and variations. *Brain Behav Evol* 26:71–80.

563 Fite KV, Kwei-Levy C, Bengston L (1989) Neurophysiological Investigation of the pretectal
564 nucleus lentiformis mesencephali in *Rana pipiens*. *Brain Behav Evol* 34:164–170.

565 Frost BJ, Wylie DR, Wang Y-C (1990) The processing of object and self-motion in the tectofugal
566 and accessory optic pathways of birds. *Vision Res* 30:1677–1688.

567 Fu Y-X, Gao H-F, Guo M-W, Wang S-R (1998) Receptive field properties of visual neurons in
568 the avian nucleus lentiformis mesencephali. *Exp Brain Res* 118:279–285.

569 Gaede AH, Baliga VB, Smyth G, Gutiérrez-Ibáñez C, Altshuler DL, Wylie DR (2022) Response
570 properties of optic flow neurons in the accessory optic system of hummingbirds versus
571 zebra finches and pigeons. *J Neurophysiol* 127:130–144.

572 Gaede AH, Goller B, Lam JPM, Wylie DR, Altshuler DL (2017) Neurons responsive to global
573 visual motion have unique tuning properties in hummingbirds. *Curr Biol* 27:279–285.

574 Gaede AH, Gutiérrez-Ibáñez C, Armstrong MS, Altshuler DL, Wylie DR (2019) Pretectal
575 projections to the oculomotor cerebellum in hummingbirds (*Calypte anna*), zebra finches
576 (*Taeniopygia guttata*), and pigeons (*Columba livia*). *J Comp Neurol* 527:2644–2658.

577 Gamlin PDR, Cohen DH (1988) Retinal projections to the pretectum in the pigeon (*Columba*
578 *livia*). *J Comp Neurol* 269:1–17.

579 Gibson JJ (1954) The visual perception of objective motion and subjective movement. *Psychol*
580 *Rev* 61:304–314.

581 Gioanni H, Rey J, Villalobos J, Dalbera A (1984) Single unit activity in the nucleus of the basal
582 optic root (nBOR) during optokinetic, vestibular and visuo-vestibular stimulations in the
583 alert pigeon (*Columba livia*). Exp Brain Res 57:49–60.

584 Gioanni H, Rey J, Villalobos J, Richard D, Dalbera A (1983) Optokinetic nystagmus in the
585 pigeon (*Columba livia*) II. Role of the pretectal nucleus of the accessory optic system
586 (AOS). Exp Brain Res 50:237–247.

587 Graf W, Simpson JI, Leonard CS (1988) Spatial organization of visual messages of the rabbit's
588 cerebellar flocculus. II. Complex and simple spike responses of Purkinje cells. J
589 Neurophysiol 60:2091–2121.

590 Grasse KL, Cynader MS (1984) Electrophysiology of lateral and dorsal terminal nuclei of the cat
591 accessory optic system. J Neurophysiol 51:276–293.

592 Gutiérrez-Ibáñez C, Wylie DR, Altshuler DL (2023) From the eye to the wing: neural circuits for
593 transforming optic flow into motor output in avian flight. J Comp Physiol A 209:839–854.

594 Hoffmann K-P, Schoppmann A (1981) A quantitative analysis of the direction-specific response
595 of neurons in the cat's nucleus of the optic tract. Exp Brain Res 42:146–157.

596 Ibbotson MR (2017) Visual neuroscience: unique neural system for flight stabilization in
597 hummingbirds. Curr Biol 27:R58–R61.

598 Ibbotson MR, Mark RF (1994) Wide-field nondirectional visual units in the pretectum: do they
599 suppress ocular following of saccade-induced visual stimulation. J Neurophysiol
600 72:1448–1450.

601 Ibbotson MR, Mark RF, Maddess TL (1994) Spatiotemporal response properties of direction-
602 selective neurons in the nucleus of the optic tract and dorsal terminal nucleus of the
603 wallaby, *Macropus eugenii*. J Neurophysiol 72:2927–2943.

604 Ibbotson MR, Price NSC (2001) Spatiotemporal tuning of directional neurons in mammalian and
605 avian pretectum: a comparison of physiological properties. J Neurophysiol 86:2621–
606 2624.

607 Iwaniuk AN, Wylie DRW (2007) Neural specialization for hovering in hummingbirds: hypertrophy
608 of the pretectal nucleus lentiformis mesencephali. J Comp Neurol 500:211–221.

609 Kano M, Kano M-S, Kusunoki M, Maekawa K (1990) Nature of optokinetic response and zonal
610 organization of climbing fiber afferents in the vestibulocerebellum of the pigmented rabbit
611 II. The nodulus. Exp Brain Res 80:238–251.

612 Karten JH, Fite KV, Brecha N (1977) Specific projection of displaced retinal ganglion cells upon
613 the accessory optic system in the pigeon (*Columba livia*). Proc Nat Acad Sci USA
614 74:1753–1756.

- 615 Kim T, Shen N, Hsiang J-C, Johnson KP, Kerschensteiner D (2020) Dendritic and parallel
616 processing of visual threats in the retina control defensive responses. *Sci Adv*
617 6:eabc9920.
- 618 Klapoetke NC, Nern A, Peek MY, Rogers EM, Breads P, Rubin GM, Reiser MB, Card GM
619 (2017) Ultra-selective looming detection from radial motion opponency. *Nature*
620 551:nature24626.
- 621 Kusunoki M, Kano M, Kano M-S, Maekawa K (1990) Nature of optokinetic response and zonal
622 organization of climbing fiber afferents in the vestibulocerebellum of the pigmented rabbit
623 I. The flocculus. *Exp Brain Res* 80:225–237.
- 624 Land MF (2015) Eye movements of vertebrates and their relation to eye form and function. *J*
625 *Comp Physiol A* 201:195–214.
- 626 Lisberger SG, Sejnowski TJ (1992) Motor learning in a recurrent network model based on the
627 vestibulo–ocular reflex. *Nature* 360:159–161.
- 628 Maddess T, Laughlin SB (1985) Adaptation of the motion-sensitive neuron H1 is generated
629 locally and governed by contrast frequency. *Proc Roy Soc B* 225:251–275.
- 630 McKenna OC, Wallman J (1985) Accessory optic system and pretectum of birds: comparisons
631 with those of other vertebrates. *Brain Behav Evol* 26:91–116.
- 632 Mustari MJ, Fuchs AF (1990) Discharge patterns of neurons in the pretectal nucleus of the optic
633 tract (NOT) in the behaving primate. *J Neurophysiol* 64:77–90.
- 634 Nixdorf-Bergweiler BE, Bischof H-J (2007) A stereotaxic atlas of the brain of the zebra finch,
635 *Taeniopygia guttata* with special emphasis on telencephalic visual and song system
636 nuclei in transverse and sagittal sections. Bethesda, MD: National Center for
637 Biotechnology Information (US). Available at:
638 <https://www.ncbi.nlm.nih.gov/books/NBK2348/>.
- 639 Pakan JMP, Graham DJ, Wylie DR (2010) Organization of visual mossy fiber projections and
640 zebrin expression in the pigeon vestibulocerebellum. *J Comp Neurol* 518:175–198.
- 641 Robinson FR, Fuchs AF (2001) The role of the cerebellum in voluntary eye movements. *Annu*
642 *Rev Neurosci* 24:981–1004.
- 643 Rodman HR, Albright TD (1987) Coding of visual stimulus velocity in area MT of the macaque.
644 *Vision Res* 27:2035–2048.
- 645 Rosenberg AF, Ariel M (1990) Visual-response properties of neurons in turtle basal optic
646 nucleus in vitro. *J Neurophysiol* 63:1033–1045.
- 647 Simpson JI (1984) The accessory optic system. *Annu Rev Neurosci* 7:13–41.
- 648 Simpson JI, Giolli RA, Blanks RH (1988a) The pretectal nuclear complex and the accessory
649 optic system. *Rev Oculomot Res* 2:335–364.

650 Simpson JI, Leonard CS, Soodak RE (1988b) The accessory optic system of rabbit. II. Spatial
651 organization of direction selectivity. *Journal of Neurophysiology* 60:2055–2072.

652 Simpson JI, Soodak RE, Hess R (1979) The accessory optic system and its relation to the
653 vestibulocerebellum. In: *Progress in Brain Research*, pp 715–724. Elsevier.

654 Smyth G, Baliga VB, Gaede AH, Wylie DR, Altshuler DL (2022) Specializations in optic flow
655 encoding in the pretectum of hummingbirds and zebra finches. *Curr Biol* 32:2772–2779.

656 Soodak RE, Simpson JI (1988) The accessory optic system of rabbit. I. Basic visual response
657 properties. *J Neurophysiol* 60:2037–2054.

658 Sun H, Frost BJ (1998) Computation of different optical variables of looming objects in pigeon
659 nucleus rotundus neurons. *Nat Neurosci* 1:296–303.

660 Vogels R, Orban GA (1994) Activity of inferior temporal neurons during orientation
661 discrimination with successively presented gratings. *J Neurophysiol* 71:1428–1451.

662 Winship IR, Crowder NA, Wylie DRW (2006) Quantitative reassessment of speed tuning in the
663 accessory optic system and pretectum of pigeons. *J Neurophysiol* 95:546–551.

664 Winterson BJ, Brauth SE (1985) Direction-selective single units in the nucleus lentiformis
665 mesencephali of the pigeon (*Columba livia*). *Exp Brain Res* 60:215–226.

666 Wylie DR (2013) Processing of visual signals related to self-motion in the cerebellum of
667 pigeons. *Front Behav Neurosci* 7.

668 Wylie DR, Frost BJ (1990) The visual response properties of neurons in the nucleus of the basal
669 optic root of the pigeon: a quantitative analysis. *Exp Brain Res* 82:327–336.

670 Wylie DR, Gaede AH, Gutiérrez-Ibáñez C, Wu P, Pilon MC, Azargoon S, Altshuler DL (2023)
671 Topography of optic flow processing in olivo-cerebellar pathways in zebra finches (
672 *Taeniopygia guttata*). *J of Comparative Neurology* 531:640–662.

673 Wylie DR, Kripalani T, Frost BJ (1993) Responses of pigeon vestibulocerebellar neurons to
674 optokinetic stimulation. I. Functional organization of neurons discriminating between
675 translational and rotational visual flow. *J Neurophysiol* 70:2632–2646.

676 Wylie DRW (2000) Projections from the nucleus of the basal optic root and nucleus lentiformis
677 mesencephali to the inferior olive in pigeons (*Columba livia*). *J Comp Neurol* 429:502–
678 513.

679 Wylie DRW, Crowder NA (2000) Spatiotemporal properties of fast and slow neurons in the
680 pretectal nucleus lentiformis mesencephali in pigeons. *J Neurophysiol* 84:2529–2540.

681

682 **Figure legends**

683 Figure 1. Experimental design for measuring direction preferences of pretectal neurons across a
684 range of stimulus speeds. A) Stimuli were shown on a single screen (84° horizontal x
685 53°vertical) that was positioned tangent to the retina. Sine wave gratings were presented in a
686 randomized order that varied in orientation and in spatial and temporal frequency. Different
687 spatial frequencies are depicted here. Each stimulus sweep consisted of 1 second of blank
688 screen, followed by 1 second of stationary stimulus presentation, and 3 seconds of stimulus
689 motion. Orientation was tested in eight directions, 45° apart. The head was pitched downward
690 45° in the stereotax. Stimulus direction is depicted relative to the orientation of a zebra finch in
691 forward flight, with 0° indicating temporal-to-nasal (TN) motion. 180° indicates nasal-to-
692 temporal, 90° indicates upward, and 270° indicates downward motion. B) A representative
693 recording from a zebra finch LM neuron in response to different speeds and directions (arrows)
694 of visual motion (green) interlaced with periods of a blank screen (white) and a stationary
695 stimulus screen (grey). Arrows indicate the orientation of the stimulus (grey), and both
696 orientation and direction (green). C) Stimulus speed is defined as the ratio of temporal to spatial
697 frequency (dashed diagonal lines). We initially tested 48 cells across a range that spanned from
698 0.062 to 1024°/s. Responses to slow speeds were minimal so we then used a narrower, but
699 more densely sampled range from 4 to 1024°/s. Inset shows the number of cells recorded at
700 each speed. In both experiments, cells were recorded at 4, 32, 256, and 1024°/s.

701 Figure 2. Representative recordings from cells at stimulus speed of 32°/s that were classified as
702 directional (A), omnidirectional (B) and bidirectional (C). Rasters from 10 sweeps in each
703 direction are aligned. Black vertical lines indicate individual spike timing. Note that directions
704 were randomized within each sweep during recording. White undershading in the raster
705 indicates the period of white screen, grey indicates static sine-wave stimulus, and green
706 indicates moving sine-wave stimulus. D-F) Corresponding polar tuning plots are shown for each
707 neuron at 32°/s. Angle indicates stimulus direction and radius indicates firing rate. The dashed
708 circle indicates the background firing rate (averaged across all static stimulus orientations) and
709 the green polynomial (mean \pm s.e.m.) is fit to data for moving stimuli. Neurons were
710 characterized using the inverse coefficient of variation (CV), sensitivity index (SI), ratio of firing
711 rate in the anti-preferred direction to that in the preferred direction (AP/PD), and peak count.

712 Figure 3. Pretectal neurons were classified in two stages using several measures of neural
713 activity. In the first stage, cells were classified as directional, bidirectional, or omnidirectional
714 based on selectivity index (SI), inverse of the coefficient of variation (CV), ratio of firing rate in
715 the anti-preferred to preferred direction (AP/PD), and peak count. A) A representative example
716 of a decision tree used by XGBoost to classify cells in the first stage is shown. This example has
717 high accuracy for the training data for which it was supplied, based on the success ratios shown
718 at the bottom. The XGBoost model was built from > 2500 decision trees. B) The relative
719 contribution (gain) and relative number of observations (cover) in the consensus model reveals
720 that SI and inverse CV were the most informative, whereas peak count and AP/PD provide
721 refinement. C) In the second stage, cells can be reclassified as unmodulated if two conditions
722 were true: i) fewer than six directions had mean firing rates that were significantly different from
723 the spontaneous rate, and ii) $SI \leq 0.29$. This step is illustrated for two cells with similar preferred
724 directions (PD) and similar activity characteristics. The upper cell is reclassified as unmodulated
725 because its activity in most directions is indistinguishable from spontaneous firing rate (grey
726 circle) and its $SI = 0.29$. The lower cell is directional even though its SI is lower because its

727 activity in six directions is above the spontaneous rate. It is not bidirectional because its SI is >
728 ~0.2. Mean spontaneous rate has been subtracted from all data and is therefore shown at 0
729 spikes/s (grey). D) A boxplot of SI values illustrates that this measurement was informative for
730 identifying directional responses. E) In contrast, inverse CV was informative for identifying
731 omnidirectional responses. Bivariate plots of inverse CV (F) and AP/PD (G) versus SI provide
732 graphical representations of how cells segregate after two stages of classification. Additional
733 detail is provided in a larger version of this figure (3-1).

734 Figure 4. Pretectal neurons are most responsive to stimulus speed of 32°/s and at this speed,
735 many cells are tuned to temporal-to-nasal (TN) motion (direction = 0°). A) Each thin line shows
736 the normalized response across directions for a single cell at a single stimulus speed. The thick
737 black line is the median response across directions for all cells tested at that speed. Speeds are
738 indicated by panel headings and color. B) The mean (\pm s.e.m.) of all cell responses across
739 directions is shown for each stimulus speed. C) A similar plot as on the left, but each cell's
740 maximum response has been aligned to 0°. D) Dots show the maximum normalized response of
741 each cell at each measured speed, regardless of direction. A cell is connected by gray lines.
742 The thick black line is the mean (\pm s.e.m.) speed tuning curve, independent of directional
743 selectivity. E) The sample size at each stimulus speed is shown by the light gray bars. Black
744 indicates the number of cells that were maximally responsive at each speed. F) Dividing the
745 black count by the light gray count provides the proportion of cells that were maximally
746 responsive at each speed.

747 Figure 5. The population of prepectal neurons shifts from a bias for directional tuning at
748 intermediate speeds to a bias for omnidirectional responses at faster speeds. A) Scatter plot of
749 preferred directions for all 924 responses. Each vertical line connects a single cell with its
750 position on the x-axis determined by its preferred direction at the speed at which it was most
751 responsive. The y-axis shows its preferred directions at all speeds at which it was tested. Size
752 of the circle corresponds to SI and color indicates classification. The bounds of gray
753 undershading are offset by $\pm 22.5^\circ$ from the line of equivalence. B) All cells were recorded at four
754 speeds: 4, 32, 256, and 1024°/s. Each response is depicted in a polar plot. The angular position
755 of each point represents a cell's direction preference, and the radial position represents SI. The
756 black circles represent SI of 0.17, above which cells tended to be directional. Example tuning
757 curves are provided for cells that were (C) directional at all four speeds, (D) shifted from
758 directional to omnidirectional, (E) omnidirectional at all four speeds, and (F) bidirectional at one
759 speed. Spontaneous rate has been subtracted from the mean response at each direction. (G) A
760 tile plot of all cell classifications at each of the four common speeds. Each row is a single cell
761 and row order is determined by classification at 32°/s. This ordering of the tile plot suggests that
762 the cells can be grouped into four categories: directional at 32°/s but omnidirectional at higher
763 speeds (H), directional at most speeds (I), omnidirectional at most speeds (J), and variable
764 across speeds (K). Whereas the polar plots in C-F are shown with the radius in spikes/s, the
765 radii of the plots in H-K are normalized to the maximum firing rate of each cell.

766 Figure 6. Individual LM neurons differ in their directional tuning across speeds. A) All 44 of the
767 LM neurons that are temporal-to-nasal preferring at 32°/s are shown. The Sankey plot illustrates
768 how the classification of these 44 cells may change at 4°/s, 256°/s, and 1024°/s. Polar plots
769 above each block contain the normalized directional tuning curves for all cells within the block.

770 B) An analogous Sankey plot is shown for the 52 LM neurons that were omnidirectionally
771 responsive at $1024^\circ/\text{s}$.

772 Figure 7. Responses in pretectal neurons are maintained throughout stimulus presentation at
773 intermediate stimulus speeds but are transient and rapid at faster speeds. A) A schematic of
774 responses (spikes/s) over three seconds (s), which is the motion epoch of the stimulus (full time,
775 FT). The response can be divided into the initial transient phase (IT, 40-200 ms), transitional
776 phase (TR, 200-1000 ms), and steady-state phase (SS, 1000-3000 ms). B) Average of
777 normalized spike rate (\pm s.e.m.) during the entire motion epoch for all cells recorded at each
778 speed. The black line indicates the average response across all directions. The green line
779 indicates the averages of the responses of each cell at the recorded direction closest to that
780 cell's preferred direction. The average response in the opposite recorded direction (180° away)
781 is shown in yellow. C) Polar plots of normalized responses for the FT, IT, TR, and SS phases.
782 Individual cell responses are normalized within each column (phase) by scaling to whichever
783 speed/direction combination had the highest activity. The thick black line is the median
784 response across directions for all cells within each polar plot. D) Averages of spike rate (\pm
785 s.e.m.) during the first 0.5 s are shown for all directions, the direction closest to the preferred
786 direction (PD), and 180° opposite to this (anti-preferred, AP). For all panels, the spontaneous
787 rate after normalization is 0 spikes/s and is shown as dotted gray lines.

788 Figure 8. The temporal response sequence of LM neurons varies with direction preference and
789 stimulus speed. The time to peak activity declines with stimulus speed both when averaged
790 across all directions (A) and when analyzed only in the direction closest to the preferred
791 direction (B). It takes longer, however, for the cells to reach peak activity when responding to
792 the preferred direction. All axes are plotted on log scales. Each dot is a single cell's response at
793 a given speed, and lines connect the same cell tested at different speeds. The thick black curve
794 (with 95% C.I. in gray) is the GAM model fit. The black horizontal line is the time that
795 corresponds to the end of the initial transient phase. Under both analytical conditions (C,D), the
796 initial transient phase peaks at higher stimulus speed than the transitional or steady-state
797 responses. Steady-state responses are generally consistent across speeds whereas the initial
798 transient and transitional phases show stronger speed-dependence. Spike rates are normalized
799 to the highest rate shown by each cell, in any direction, across the full motion epochs.

800

801 **Tables**

Formula	R ²	Root mean squared error	Sigma	AIC
$R_n \sim (1 cell)$	0	0.36	0.36	756.23
$R_n \sim s(\log_2(speed))$	0.52	0.25	0.25	135.58
$R_n \sim s(\log_2(speed)) + (1 cell)$	0.52	0.25	0.25	137.26

802 Table 1. Goodness of fit metrics for models fit to explain normalized directional response (R_n).
803 Three GAM models were fit, with potential explanatory variables including \log_2 of stimulus speed
804 ($speed$) and cell identity ($cell$; as a random effect). Sigma column denotes the residual standard
805 deviation. The best-fitting model, determined by lowest AIC score, is in bold.

Formula	R2	Root mean squared error	Sigma	AIC
$\log_2(time_p) \sim (1 cell)$	0.17	1.45	1.52	2749.10
$\log_2(time_p) \sim s(\log_2(speed))$	0.42	0.96	1.04	2414.84
$\log_2(time_p) \sim s(\log_2(speed)) + (1 cell)$	0.42	0.96	1.04	2308.35
$\log_2(time_p) \sim s(\log_2(speed) * shape)$	0.41	1.27	1.28	2436.73
$\log_2(time_p) \sim s(\log_2(speed) * shape) + (1 cell)$	0.41	0.96	1.04	2334.81

806 Table 2. Goodness of fit metrics for models fit to explain \log_2 of time to peak response ($time_p$).
807 Data come from averaged responses across all directions for each cell, at each speed. Five
808 GAM models were fit, with potential explanatory variables including \log_2 of stimulus speed
809 ($speed$), shape category ($shape$; directional, omnidirectional or bidirectional), and cell identity
810 ($cell$; as a random effect). Sigma column denotes the residual standard deviation. The best-
811 fitting model, determined by lowest AIC score, is in bold.

Formula	R2	Root mean squared error	Sigma	AIC
$\log_2(time_p) \sim (1 cell)$	0.21	1.46	1.54	2331.51
$\log_2(time_p) \sim s(\log_2(speed))$	0.00	1.48	1.48	2198.54
$\log_2(time_p) \sim s(\log_2(speed)) + (1 cell)$	0.26	1.20	1.28	2136.02
$\log_2(time_p) \sim s(\log_2(speed) * shape)$	0.00	1.47	1.48	2213.71

$\log_2(\text{time}_p) \sim s(\log_2(\text{speed}) * \text{shape}) + (1 \text{cell})$	0.27	1.18	1.27	2152.49
---	------	------	------	---------

812 Table 3. Goodness of fit metrics for models fit to explain \log_2 of time to peak response (time_p).
813 Data come from only the direction closest to the preferred direction for each cell, at each speed.
814 Five GAM models were fit, with potential explanatory variables including \log_2 of stimulus speed
815 (speed), shape category (shape ; directional, omnidirectional or bidirectional), and cell identity
816 (cell ; as a random effect). Sigma column denotes the residual standard deviation. The best-
817 fitting model, determined by lowest AIC score, is in bold.

Formula	R2	Root mean squared error	Sigma	AIC
$\text{activity}_p \sim (1 \text{cell})$	0.15	0.13	0.14	-2419.55
$\text{activity}_p \sim \text{phase} + s(\log_2(\text{speed}) * \text{phase})$	0.21	0.10	0.11	-3465.61
$\text{activity}_p \sim \text{phase} + s(\log_2(\text{speed}) * \text{phase}) + (1 \text{cell})$	0.41	0.09	0.94	-3922.36

818 Table 4. Goodness of fit metrics for models fit to explain magnitude of peak activity within each
819 phase (activity_p). Data come from averaged responses across all directions for each cell, at
820 each speed. Three GAM models were fit, with potential explanatory variables including \log_2 of
821 stimulus speed (speed), phase category (phase ; initial transient, transitional, or steady state),
822 and cell identity (cell ; as a random effect). Sigma column denotes the residual standard
823 deviation. The best-fitting model, determined by lowest AIC score, is in bold.

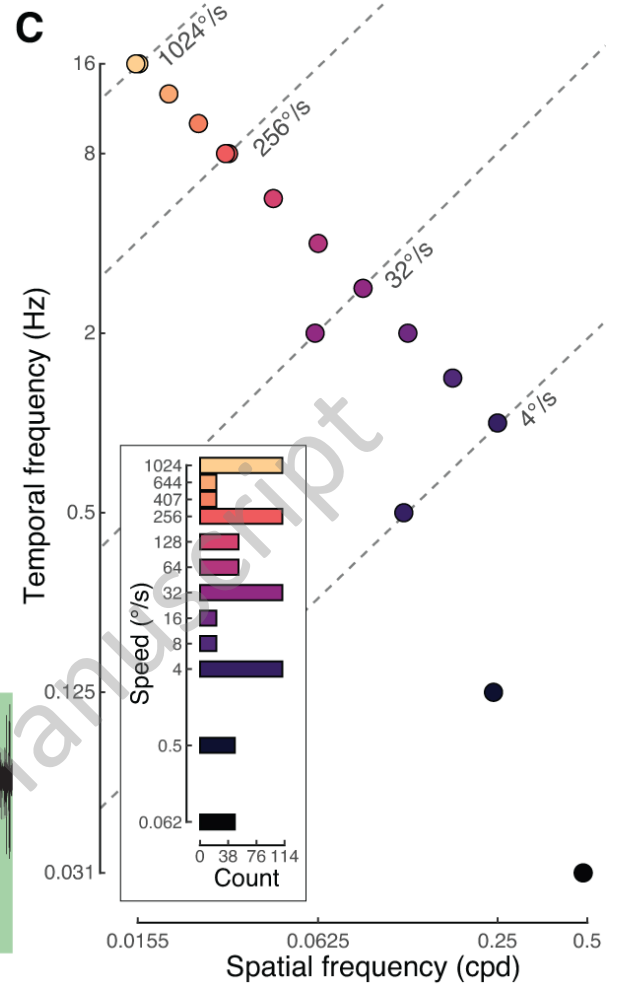
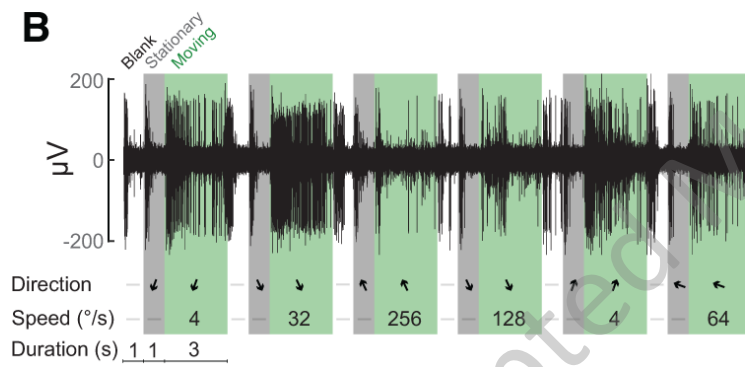
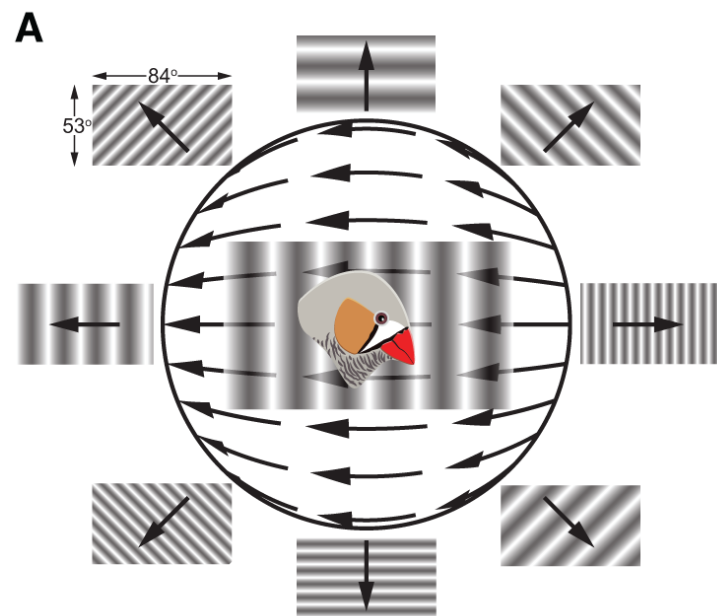
Formula	R2	Root mean squared error	Sigma	AIC
$\text{activity}_p \sim (1 \text{cell})$	0.16	0.20	0.21	-527.77
$\text{activity}_p \sim \text{phase} + s(\log_2(\text{speed}) * \text{phase})$	0.03	0.19	0.19	-1059.27
$\text{activity}_p \sim \text{phase} + s(\log_2(\text{speed}) * \text{phase}) + (1 \text{cell})$	0.21	0.17	0.17	-1317.23

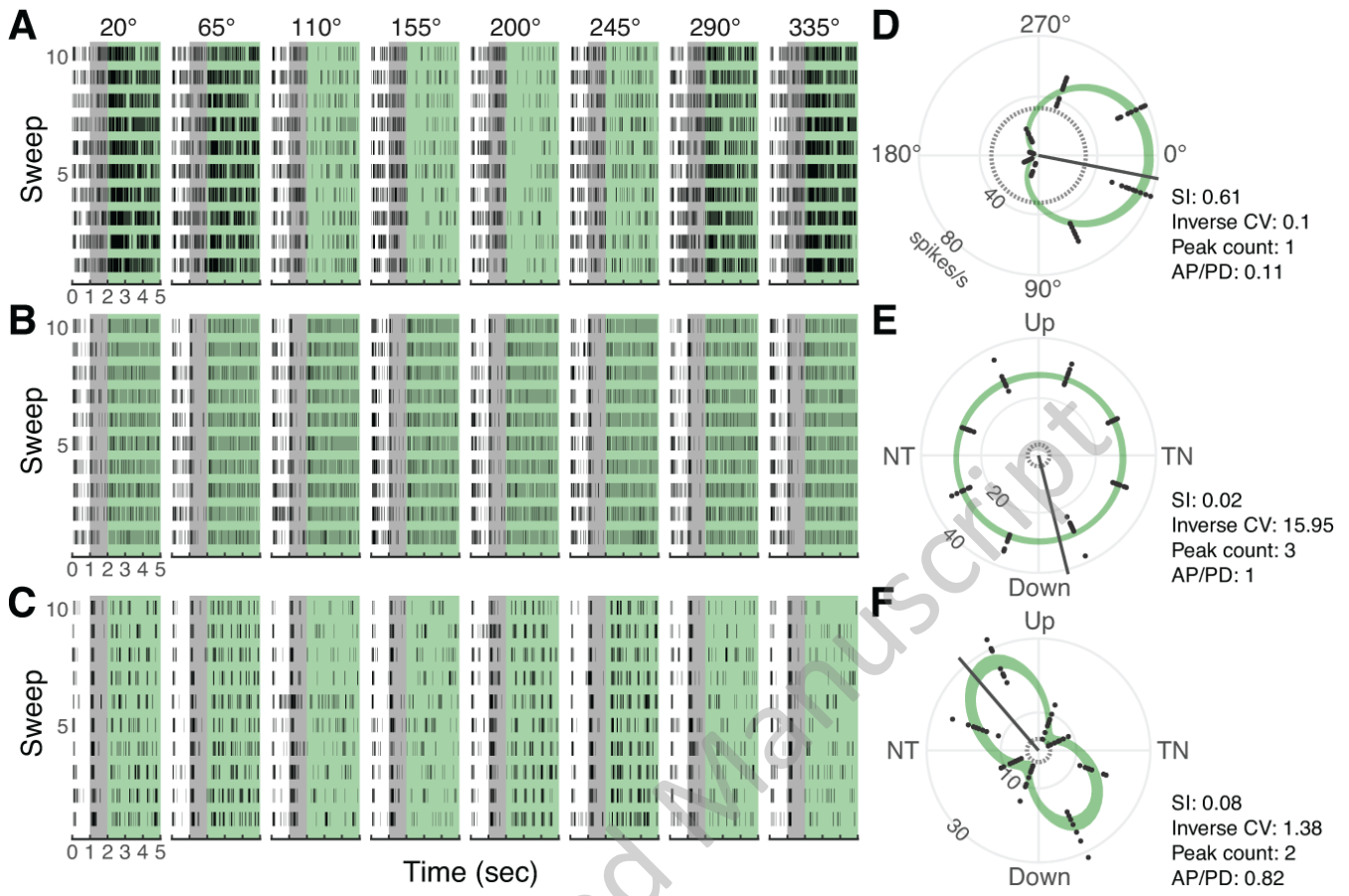
824 Table 5. Goodness of fit metrics for models fit to explain magnitude of peak activity within each
825 phase (activity_p). Data come from only the direction closest to the preferred direction for each
826 cell, at each speed. Three GAM models were fit, with potential explanatory variables including
827 \log_2 of stimulus speed (speed), phase category (phase ; initial transient, transitional, or steady
828 state), and cell identity (cell ; as a random effect). Sigma column denotes the residual standard
829 deviation. The best-fitting model, determined by lowest AIC score, is in bold.

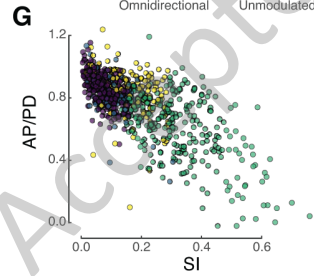
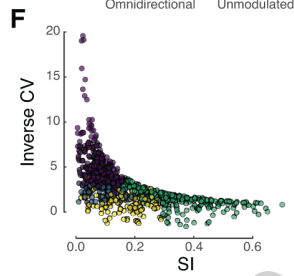
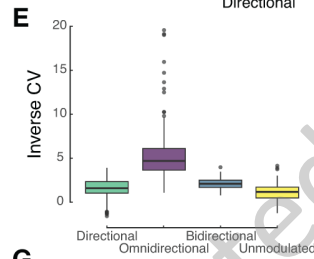
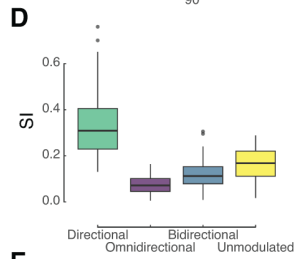
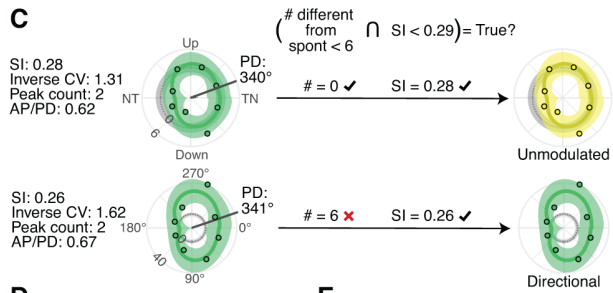
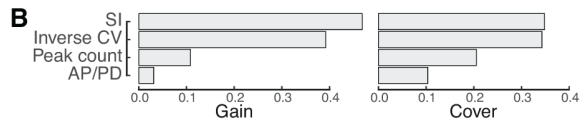
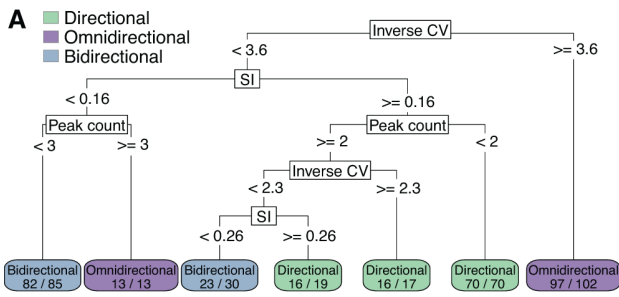
Data structure	Type of test	Power
Categorical (cell shape categories)	Chi-square	DF: 426, $p < 0.001$

831 Table 6. Summary of formal hypothesis testing conducted. DF = degrees of freedom.

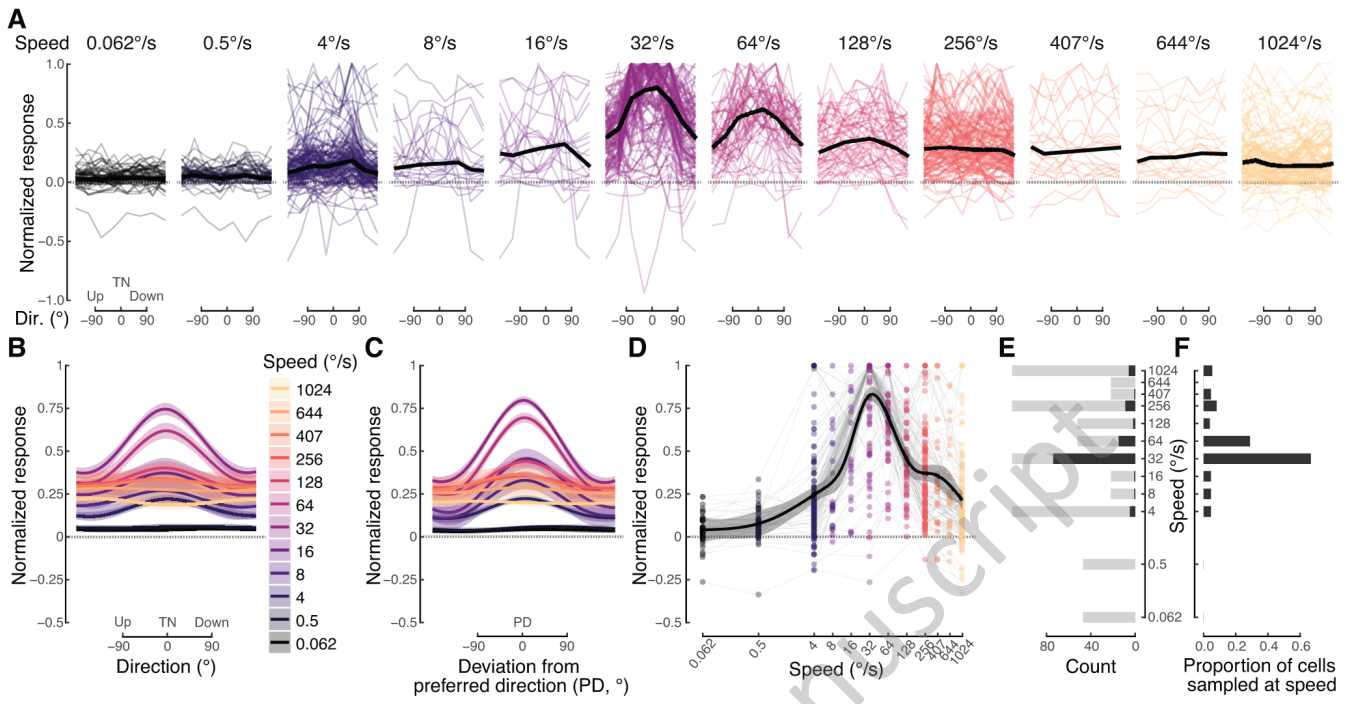
eNeuro Accepted Manuscript

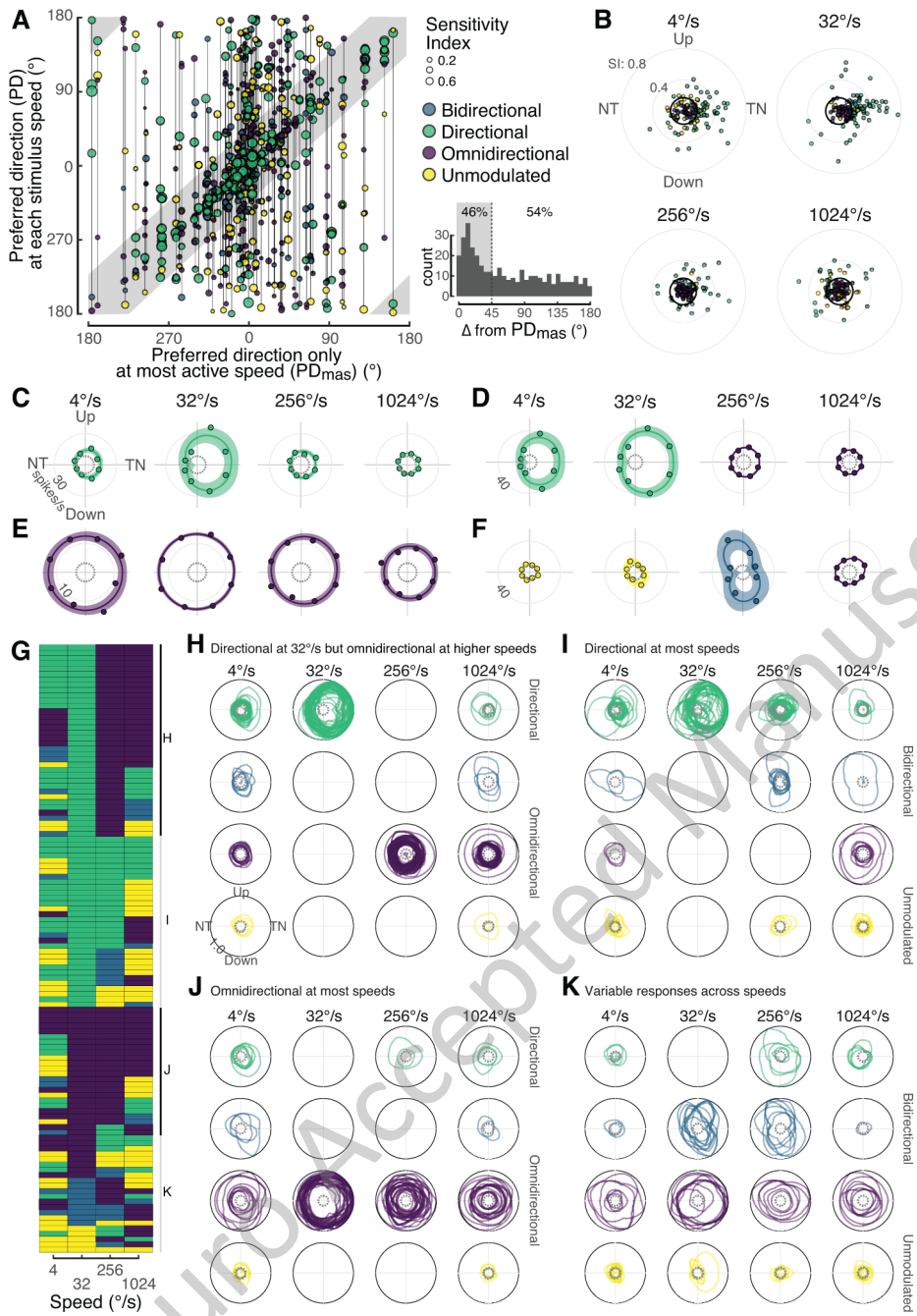


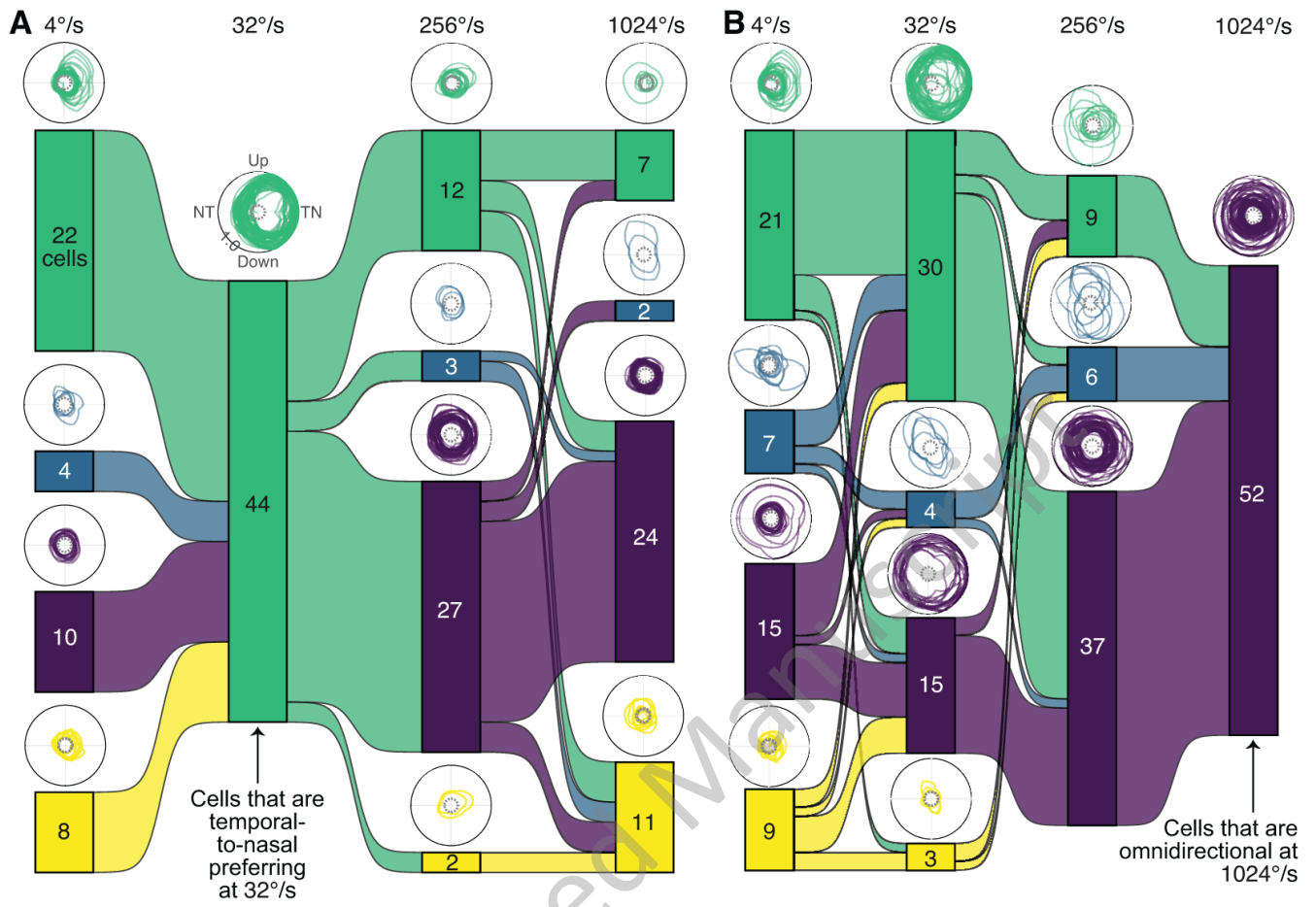




eNeuro Accepted Manuscript







eNeuro Accepted Manuscript

